# 6G-INTEGRATION-01-E5: Broadband detector

## 6G-INTEGRATION

Full Title: Construction of an ecosystem for research and development in non-terrestrial networks (satellite and HAPS) and B5G (3GPP rel. 17 and beyond): NTN networks for LEO satellites and for HAPS platforms.

Program: UNICO 5G I+D 2021

Start date: Jan 1, 2024 End date: Dec 31, 2024

Duration: 12 months



Financiado por la Unión Europea NextGenerationEU
Plan de Recuperación, Transformación y Resiliencia

| | |
|---|---|
| **Document type** | Deliverable |
| **Document Id** | 6G-INTEGRATION-01-E5 |
| **Document title** | Broadband detector |
| **Document responsible** | Sandra Santiago (UC3M) |
| **Document editor** | Sandra Santiago (UC3M) |
| **Receiver** | Daniel Segovia (UC3M; 6G-INTEGRATION Principal Investigator) |
| **Contributors** | Sandra Santiago, Alejandro Rivera, Elizabeth Fernández |

| | |
|---|---|
| **Version** | 1.0 |
| **Planned Due date** | December 31, 2024 |
| **Actual submission date** | December 10, 2024 |

Financiado por la Unión Europea NextGenerationEU
GOBIERNO DE ESPAÑA MINISTERIO DE ASUNTOS ECONÓMICOS Y TRANSFORMACIÓN DIGITAL SECRETARÍA DE ESTADO DE TELECOMUNICACIONES E INFRAESTRUCTURAS DIGITALES
Plan de Recuperación, Transformación y Resiliencia
UNICO I+D

uc3m

## Executive Summary

*This document provides a detailed description of the solution implemented by UC3M for the 6G-Integration project, aimed at developing an ultrawideband broadband detector.*

*The development of broadband receivers is closely aligned with the objectives of 3GPP Release 17 ("Rel17"), which introduces standardized support for Non-Terrestrial Networks (NTNs) within the 5G framework. These networks, encompassing Low Earth Orbit (LEO) satellites and High-Altitude Platform Stations (HAPS) platforms, demand highly flexible and adaptive receiver architectures capable of operating across wide frequency ranges to address the diverse spectrum allocations, dynamic channel conditions, and Doppler effects inherent to NTN scenarios. Broadband receivers enable critical functionalities such as carrier aggregation across disparate bands, efficient spectrum utilization, and dynamic adaptation to varying propagation environments. As such, they are key enablers for the implementation of Rel17 NTN features and form a foundational technology for the evolution toward beyond 5G (B5G) and 6G, where integration of terrestrial and non-terrestrial systems and exploitation of higher frequency bands will be essential.*

*UC3M's proposal is based on a high-sensitivity THz photon counting receiver operating in the 75-110 GHz band. The receiver is based on a Whispering Gallery Mode Resonator (WGMR) and a dielectric rod waveguide (DRW) antenna for efficient coupling of THz power to the resonator.*

*This report focuses on the development of the broadband DRW antenna. Both the design process and the experimental validation of a manufactured prototype are presented.*

Financiado por la Unión Europea NextGenerationEU
GOBIERNO DE ESPAÑA MINISTERIO DE ASUNTOS ECONÓMICOS Y TRANSFORMACIÓN DIGITAL SECRETARÍA DE ESTADO DE TELECOMUNICACIONES E INFRAESTRUCTURAS DIGITALES
Plan de Recuperación, Transformación y Resiliencia
UNICO I+D

## Resumen ejecutivo

Este documento ofrece una descripción detallada de la solución implementada por la UC3M en el marco del proyecto 6G-Integration, cuyo objetivo es el desarrollo de un detector de banda ultraancha.

El desarrollo de receptores de banda ancha está estrechamente alineado con los objetivos de la Release 17 del 3GPP ("Rel17"), que introduce el soporte estandarizado para las Redes No Terrestres (NTN) dentro del ecosistema 5G. Estas redes, que incluyen satélites en órbita baja (LEO) y plataformas de gran altitud (HAPS), requieren arquitecturas de receptor altamente flexibles y adaptativas, capaces de operar en rangos de frecuencia amplios para abordar la diversidad en la asignación espectral, las condiciones dinámicas del canal y los efectos Doppler propios de los escenarios NTN.Los receptores de banda ancha permiten funcionalidades clave como la agregación de portadoras en bandas no contiguas, el uso eficiente del espectro y la adaptación dinámica a entornos de propagación variables. Por tanto, constituyen una tecnología habilitadora esencial para la implementación de las funcionalidades NTN definidas en Rel17, y sientan las bases para la evolución hacia B5G y 6G, donde la integración de redes terrestres y no terrestres, así como el aprovechamiento de bandas de frecuencia más altas, será fundamental.

La propuesta de la UC3M se basa en un receptor de conteo de fotones en terahercios (THz) de alta sensibilidad, operando en la banda de 75–110 GHz. El receptor emplea un resonador de modo galería de susurros (WGMR) y una antena de guía de onda de varilla dieléctrica (DRW) para lograr un acoplamiento eficiente de la potencia en THz al resonador.

Este informe se centra en el desarrollo de una antena DRW de banda ancha para este receptor, presentándose los detalles de diseño y validación experimental de un prototipo de esta en las siguientes secciones.

Financiado por la Unión Europea NextGenerationEU
GOBIERNO DE ESPAÑA MINISTERIO DE ASUNTOS ECONÓMICOS Y TRANSFORMACIÓN DIGITAL SECRETARÍA DE ESTADO DE TELECOMUNICACIONES E INFRAESTRUCTURAS DIGITALES
Plan de Recuperación, Transformación y Resiliencia
UNICO I+D

uc3m

# Contents



Financiado por la Unión Europea NextGenerationEU
GOBIERNO DE ESPAÑA MINISTERIO DE ASUNTOS ECONÓMICOS Y TRANSFORMACIÓN DIGITAL SECRETARÍA DE ESTADO DE TELECOMUNICACIONES E INFRAESTRUCTURAS DIGITALES
Plan de Recuperación, Transformación y Resiliencia
UNICO I+D

## List of Figures

## Glossary

| | |
|---|---|
| 3GPP | 3rd Generation Partnership Project |
| 5G | 5th Generation technology standard for cellular networks |
| 6G | 6th Generation technology standard for cellular networks |
| AE | Antenna Emitter |
| B5G | Beyond 5G |
| DRW | Dielectric Rod Waveguide |
| HAPS | High Altitude Platform Station |
| LEO | Low Earth Orbit |
| mmWave | Millimeter waves |
| NF | Near Field |
| NTN | Non-Terrestrial Network |
| Rel17 | Release 17 of the 5G standar |
| THz | Terahertz |
| UC3M | Universidad Carlos III de Madrid |
| WGMR | Whispering Gallery Mode Resonator |
| WR | Waveguide Rectangular |
| XPD | Cross-polar discrimination |

Financiado por la Unión Europea NextGenerationEU
GOBIERNO DE ESPAÑA MINISTERIO DE ASUNTOS ECONÓMICOS Y TRANSFORMACIÓN DIGITAL SECRETARÍA DE ESTADO DE TELECOMUNICACIONES E INFRAESTRUCTURAS DIGITALES
Plan de Recuperación, Transformación y Resiliencia
UNICO I+D

# 1 Introduction

The integration of terrestrial and non-terrestrial networks (NTNs) represents a fundamental step toward the realization of global, ubiquitous connectivity in future 5G and beyond-5G (B5G/6G) systems. 3GPP Release 17 (Rel17) marks a significant milestone by introducing standardized support for NTNs within the 5G architecture, enabling seamless interoperability between ground-based infrastructure and platforms such as Low Earth Orbit (LEO) satellites and High-Altitude Platform Stations (HAPS). This evolution brings about new challenges in terms of system design, particularly at the radio frequency front-end, where communication links must adapt to a wide variety of propagation environments, spectrum allocations, and mobility patterns.

In this context, the development of broadband receiver technologies is of critical importance. These receivers must operate across ultra-wide frequency bands to support flexible spectrum use, carrier aggregation, and the coexistence of multiple services and waveforms. Moreover, the unique conditions of NTN links—such as large Doppler shifts, long signal delays, and high path losses—demand receiver architectures with high sensitivity, low noise figures, and strong adaptability. Broadband receivers thus serve as key enablers for the successful implementation of NTN capabilities defined in Rel17, being essential for future evolutions of the 5G standard toward fully integrated terrestrial and non-terrestrial systems.

A high-sensitivity receiver in the range from 75 to 110 GHz has been developed at UC3M for ultra-wide band operation. Figure 1 shows the schematic of the proposed receiver, which is formed by a Dielectric Rod Waveguide Antenna (DRWA) and a Whispering Gallery Mode Resonator (WGMR) for efficient coupling of the THz power.

This document focuses on the design of the radiating part of the DRWA. Different illumination strategies are analysed to achieve broadband operation, and a prototype of the final design is manufactured for experimental validation.

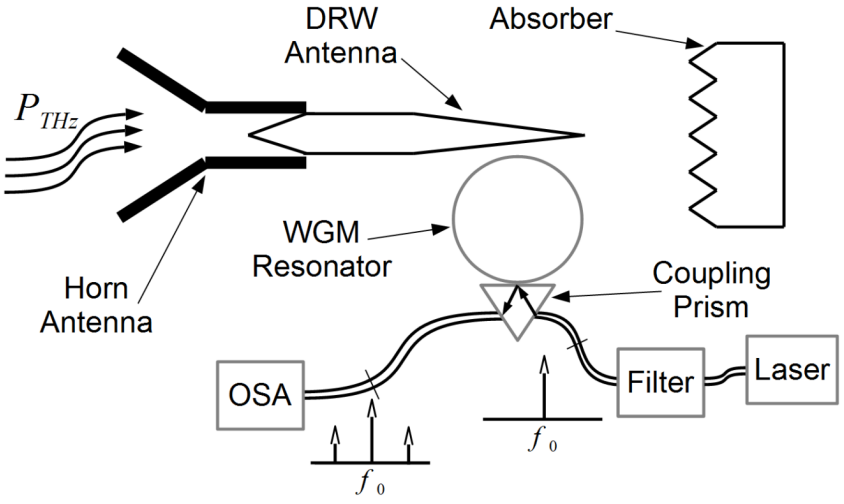


*Figure 1 – Schematic of the proposed broadband receiver*

# 2 Dielectric ROD Antenna

Dielectric Rod Waveguide (DRW) antennas consist of a high-permittivity dielectric rod that acts as a waveguide for electromagnetic waves. DRW antennas are widely used in high-frequency systems, including millimeter-wave (mmWave) and terahertz (THz) applications, due to their simple structure, low cost, compactness and ease of integration with other active and passive devices.

Despite the lack of analytical solutions for calculating the structure modes, DRWs with a rectangular cross-section are considered since its ease of manufacture makes them cost affordable even when using high-permittivity materials such as silicon and GaAs ($\varepsilon_{sc} \approx 12$).

Marcatilli's approximation is used to approximate the propagation constant and optimize the width and thickness of the rod ($W_{ROD} = 0.5\ mm, THK = 0.5\ mm$) to achieve single propagation of the $E_{11}^{x}$ mode in the 75-110 GHz frequency range.

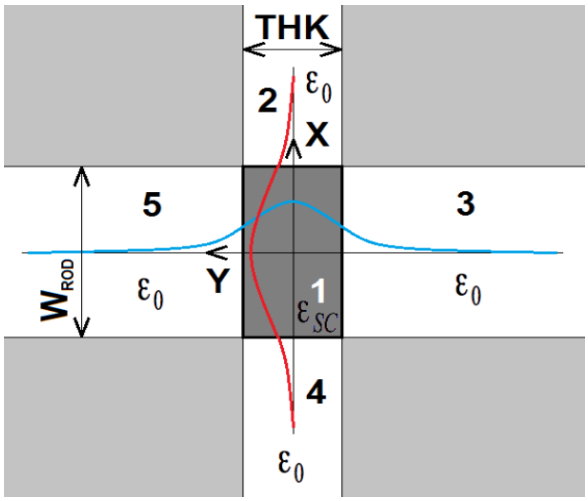


*Figure 2 – Cross section of the rectangular DRW*

# 3 Feeding of the DRA

Two different illumination strategies are analyzed to feed the DRW. First, the use of rectangular waveguides is proposed as they are easy to implement. Then, antenna emitters (AE) are analyzed to achieve higher THz power extraction from the high permittivity substrate. This section provides a more detailed explanation of these strategies, and the limitations observed in each of them.

## 3.1 Rectangular waveguide feeding

The sketch of a DRW fed through a rectangular waveguide is presented in Figure 3a, where two additional tapers are added at both sides of the DRW to achieve both good matching in the operation band and proper radiation to the free space.

The manufactured prototype of these antenna is presented in Figure 3b. The dimensions of the tapers are optimized ($L_{TAPER}$ = 8 mm, $L_{RAD}$ = 15 mm) for its operation at 100 GHz while covering the full WR-10 operation band. Proper alignment into the metal waveguide is achieved by gluing a low-density foam ring in a 2 mm long section of the DRW, while contact between metal and semiconductor is avoided using a Teflon strip. The maximum cross section of the proposed DRW antenna is 0.5x1.0mm.

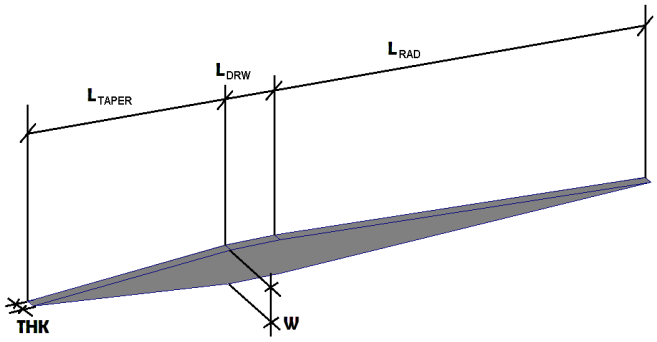


*(a)*

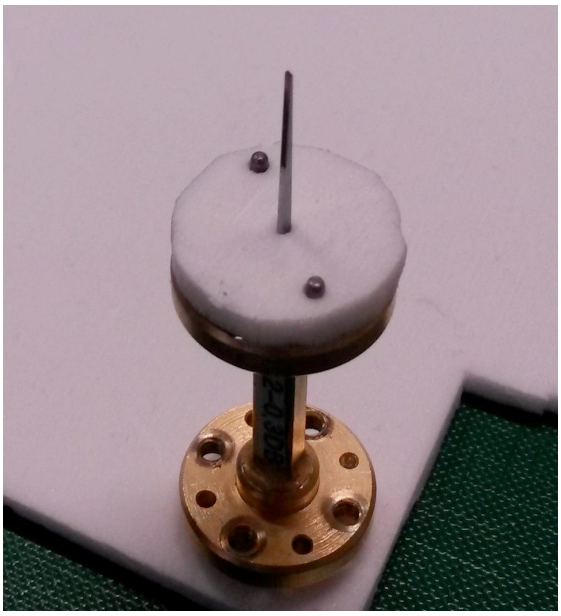

*(b)*

*Figure 3 – Dielectric rod waveguide antenna. (a) Sketch, (b) Manufactured prototype at 100 GHz fed with a WR-10.*

Efficient feeding through the waveguide is observed in the E-field distributions presented in Figure 4, where the field is predominantly guided into the DRW, and single-mode propagation is achieved. This is consistent with the experimental reflection S-parameters shown in Figure 5, where a good matching (below 15 dB) is appreciated in the whole operation band (75-110 GHz).

Financiado por la Unión Europea NextGenerationEU
GOBIERNO DE ESPAÑA MINISTERIO DE ASUNTOS ECONÓMICOS Y TRANSFORMACIÓN DIGITAL SECRETARÍA DE ESTADO DE TELECOMUNICACIONES E INFRAESTRUCTURAS DIGITALES
Plan de Recuperación, Transformación y Resiliencia
UNICO I+D

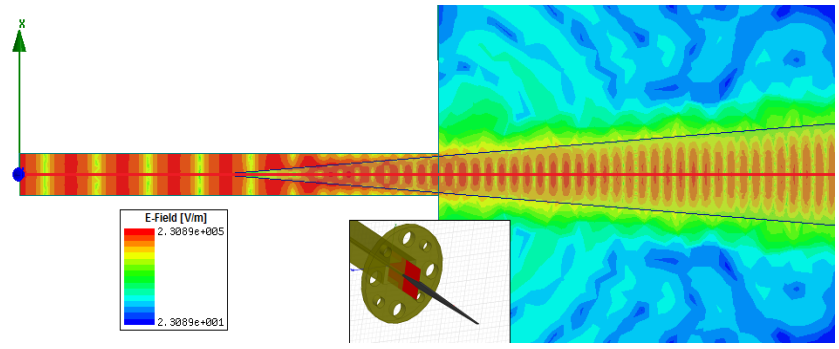


*(a)*

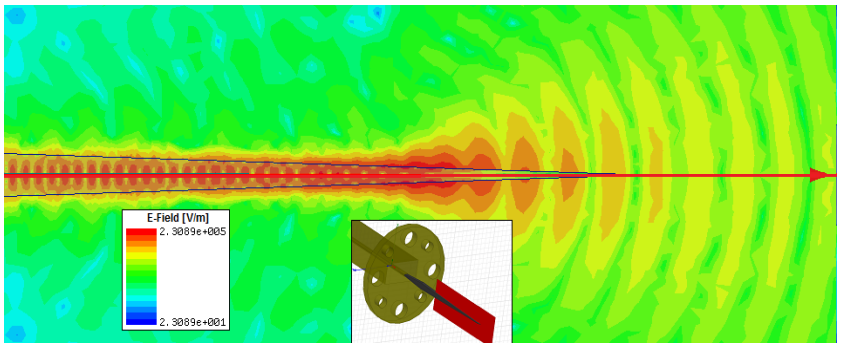


*(b)*

*Figure 4 – Simulated E-field distribution [log(V/m)] on XZ plane in the DRW*

*(a) Waveguide DRW transition, (b) radiation taper*

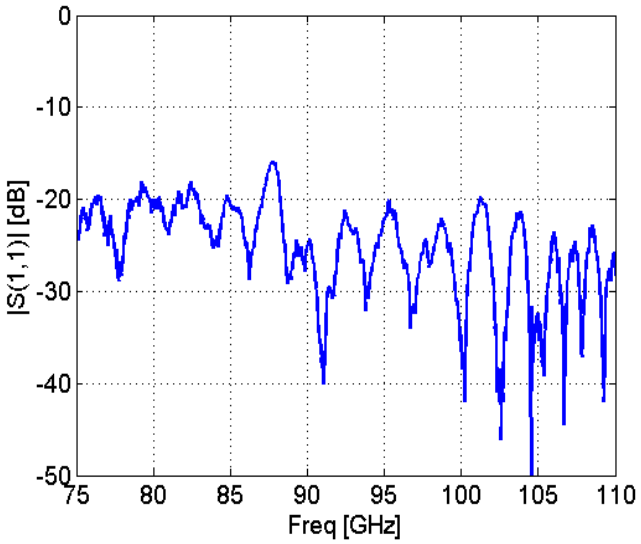


*Figure 5 – Measured S11 of the DRW antenna fed through a waveguide*

Good agreement is achieved between the simulated (dashed) and measured (solid) radiation patterns, as can be seen in Figure 6. A gain of 16 dB is measured, with a cross-polar discrimination (XPD) of 28 dB in the main lobe direction.

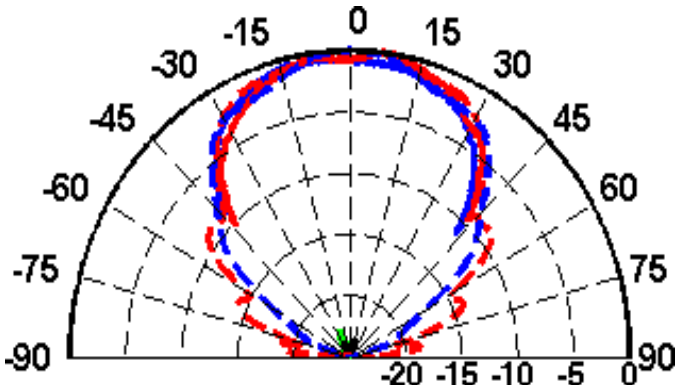


*Figure 6 – Simulated (dashed) and measured (solid) radiation of the DRW antenna.*

*E-plane (ϕ = 0°, red) and H-plane (ϕ = 90°, blue).*

## 3.2 Antenna emitter feeding

The schematic of a DRW antenna fed by an AE THz source is presented in *Figure 7*. An E-field X-axis direction for the fundamental mode inside the DRW is considered to achieve efficient illumination, and an X-axis oriented linearly polarized log-periodic antenna is placed to avoid a 3-dB penalization. Reflection losses in the discontinuity are prevented by using the same permittivity for the semiconductor and the DRW ($\varepsilon_{sc} = \varepsilon_{DRW}$).

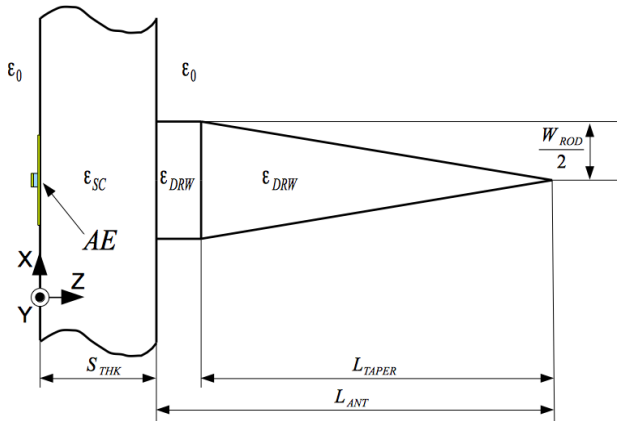


*Figure 7 – Sketch of the dielectric antenna fed through an AE.*

First, a proof-of-concept of this approach based on an already available DRW antenna is developed. Figure 8 depicts the prototype of this antenna manufactured on a 0.6 mm thick low-loss semi-insulating GaAs wafer. $L_{TAPER}$ and $W_{ROD}$ are defined as 8 and 1.2 mm, respectively, and a 15 mm long dielectric rectangular waveguide is placed between the radiation taper and the wafer. A three-period *n-i-pn-i-p* photomixer manufactured in a InP wafer of 0.4 mm

Financiado por la Unión Europea NextGenerationEU
GOBIERNO DE ESPAÑA MINISTERIO DE ASUNTOS ECONÓMICOS Y TRANSFORMACIÓN DIGITAL
SECRETARÍA DE ESTADO DE TELECOMUNICACIONES E INFRAESTRUCTURAS DIGITALES
Plan de Recuperación, Transformación y Resiliencia
UNICO I+D

thickness is attached to the log-periodic antenna, and an RC filter is added to protect the AE from electrostatic shocks.

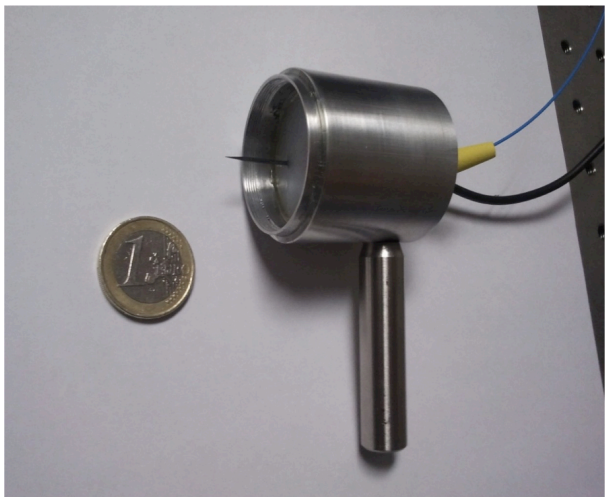

*Figure 8 – Proof-of-concept prototype of an AE with a DRW antenna.*

Figure 9 compares the radiation pattern at 137 GHz of the DRW antenna with the one obtained with a 10 mm diameter silicon lens instead. Lower power is achieved with the DRW, while a slight tilt due to misalignment between the lens and the AE is observed in the E-plane.

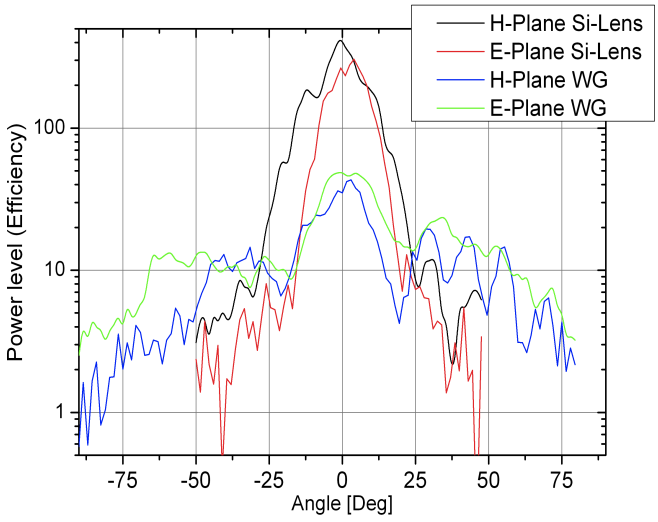


*Figure 9 – Comparison between measured power using a silicon lens and DRW antenna.*

The dimensions of this antenna are optimized ($L_{TAPER}$ = 8 mm, $W_{ROD}$ = 0.5 mm) to achieve operation at 200 GHz. A second prototype is manufactured in a low-loss high-resistivity silicon wafer with a thickness of 0.5 mm is used. Radiation in the union is avoided by coupling the wafer and the DRW in the near field (NF) as illustrated in *Figure 10*, and the RC roll-off is reduced by using a three-period InGaAs *n-i-pn-i-p* photomixer with a log-periodic antenna.

Financiado por la Unión Europea NextGenerationEU
GOBIERNO DE ESPAÑA MINISTERIO DE ASUNTOS ECONÓMICOS Y TRANSFORMACIÓN DIGITAL SECRETARÍA DE ESTADO DE TELECOMUNICACIONES E INFRAESTRUCTURAS DIGITALES
Plan de Recuperación, Transformación y Resiliencia
UNICO I+D

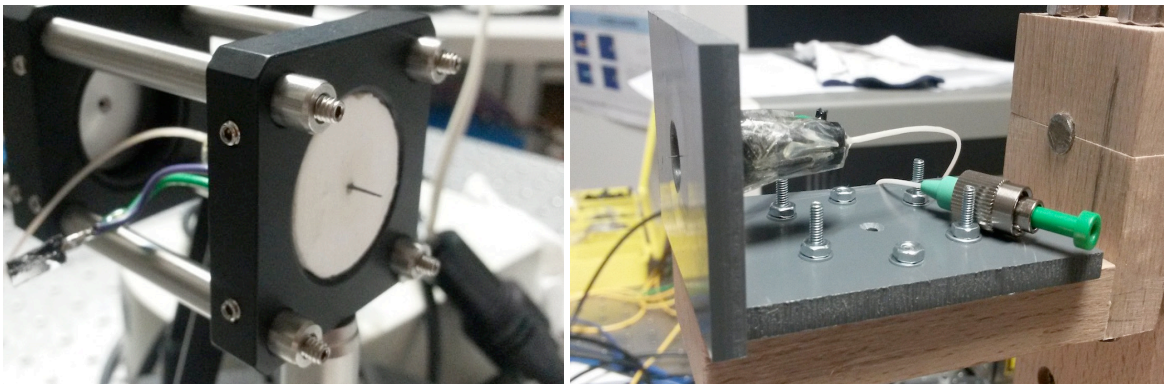

*Figure 10 - Assembly of the prototype of the DRW coupled in the NF to the AE.*

The radiation pattern of this antenna is measured with a non-coherent scheme detector based on a Golay cell, an optical chopper and a locking amplifier. A poor dynamic range (12 dB) is achieved, leading in a photocurrent lower than expected (150 nA). A maximum tolerance of $\pm$ 100 $\mu$m is required in the DRW antenna alignment for the XY plane for efficient coupling of the THz power to the fundamental mode of the rod.

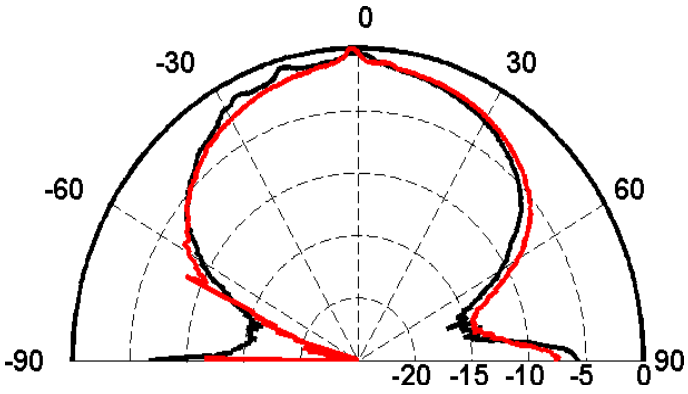


*Figure 11 – Measured radiation pattern at 150 GHz of the DRW + AE.*

*E-plane (XZ plane, black) and H-plane (YZ plane,red)*

Figure 12 show the E-field distributions inside the DRW antenna at different frequencies. Multi-mode propagation is observed at higher frequencies, where $W_{ROD}$ is electrically large. This compromises the bandwidth of the DRW as a multilobe radiation pattern is achieved due to the presence of widely dispersed radiation zones through the rod axis.

Financiado por la Unión Europea NextGenerationEU
GOBIERNO DE ESPAÑA MINISTERIO DE ASUNTOS ECONÓMICOS Y TRANSFORMACIÓN DIGITAL
SECRETARÍA DE ESTADO DE TELECOMUNICACIONES E INFRAESTRUCTURAS DIGITALES
Plan de Recuperación, Transformación y Resiliencia
UNICO I+D

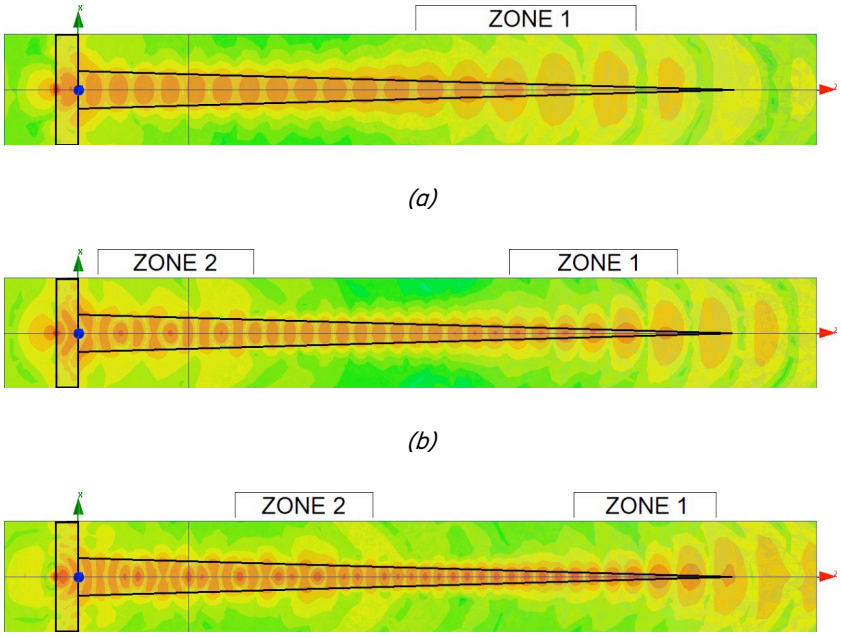


*Figure 12 – Simulated E-field distribution [log(V/m)] on XZ plane of the DRW + AE*

*(a) 200 GHz, (b) 250 GHz, and (c) 300 GHz*

# 4 Ultra-wideband DRW antenna

In order to overcome the bandwidth limitations of DRW antennas due to higher-order modes, a planar lens is introduced as shown in Figure 13 to rectify the generated wavefront of the spherical waves.

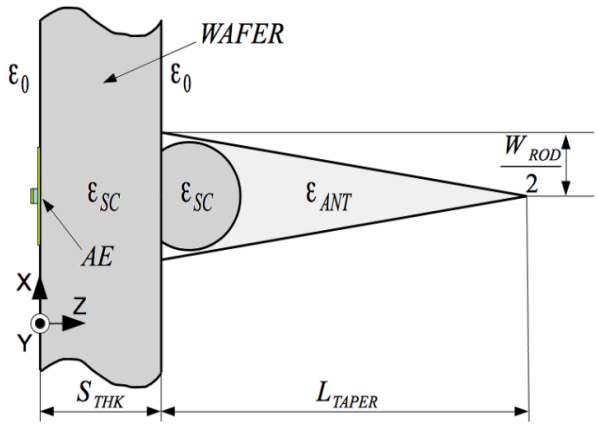


Figure 13 - Sketch of dielectric rod waveguide antenna with an embedded planar lens

Financiado por la Unión Europea NextGenerationEU
GOBIERNO DE ESPAÑA MINISTERIO DE ASUNTOS ECONÓMICOS Y TRANSFORMACIÓN DIGITAL
SECRETARÍA DE ESTADO DE TELECOMUNICACIONES E INFRAESTRUCTURAS DIGITALES
Plan de Recuperación, Transformación y Resiliencia
UNICO I+D

Reflection losses are minimized by fixing the radiation taper permittivity $\varepsilon_{ant}$ to an intermediate value between $\varepsilon_{sc}$ and $\varepsilon_0$. The lens is E-plane oriented to minimize reflections in the refractive interface, and its dimensions are chosen to collect most of the THz power while the critical angle is greater than the AE beam waist. Exact and approximated solutions are studied by integrating elliptical and hyper-hemispheric lenses in a DRW antenna of dielectric constant $\varepsilon_{ant}$ = 3.5, rod length $L_{TAPER}$ =17 mm and width $W_{ROD}$ = 2.2 mm, and equal thickness for the wafer and the DRW ($THK = 300\ \mu$m).

## 4.1 Elliptical lens

The geometry of the embedded elliptical planar lens analyzed is presented in Figure 14. The AE is placed in one of the ellipses focus at 1.5 mm from the refractive surface along the Z-axis.

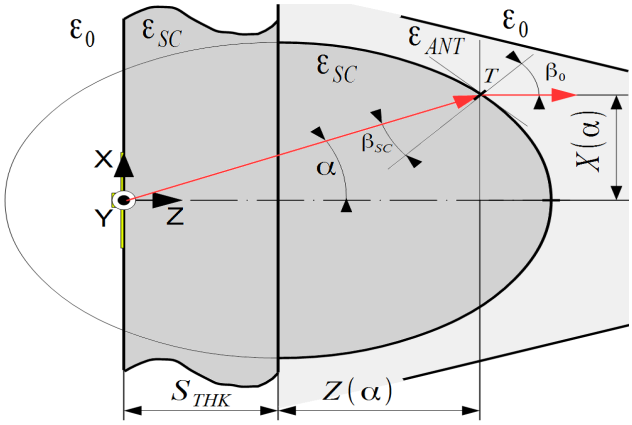


Figure 14 – Geometry of the embedded elliptical planar lens

The E-field distributions presented in Figure 15 demonstrate that the introduction of an elliptic lens transforms the generated spheric wave reducing excitation of higher order in the DRW, even for higher frequencies on which the rod is electrically large. Although this reduces the secondary radiation zones along the antenna, side lobes are still visible at higher frequencies in the radiation patterns included in Figure 16.

Financiado por la Unión Europea NextGenerationEU
GOBIERNO DE ESPAÑA MINISTERIO DE ASUNTOS ECONÓMICOS Y TRANSFORMACIÓN DIGITAL
SECRETARÍA DE ESTADO DE TELECOMUNICACIONES E INFRAESTRUCTURAS DIGITALES
Plan de Recuperación, Transformación y Resiliencia
UNICO I+D

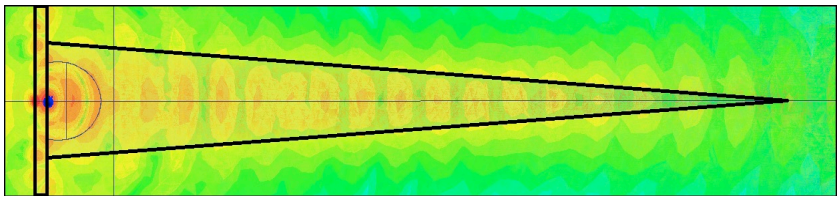

*(a)*

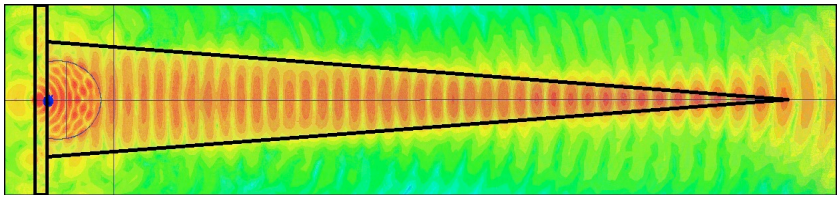

*(b)*

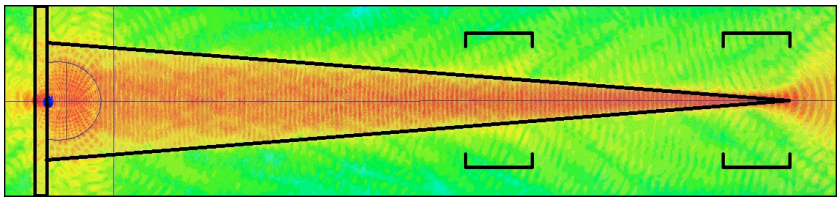

*(c)*

*Figure 15 – Simulated E-field distribution [log(V/m)] on XZ plane for an elliptic lens at (a) 150 GHz, (b) 300 GHz, (c) 800 GHz*

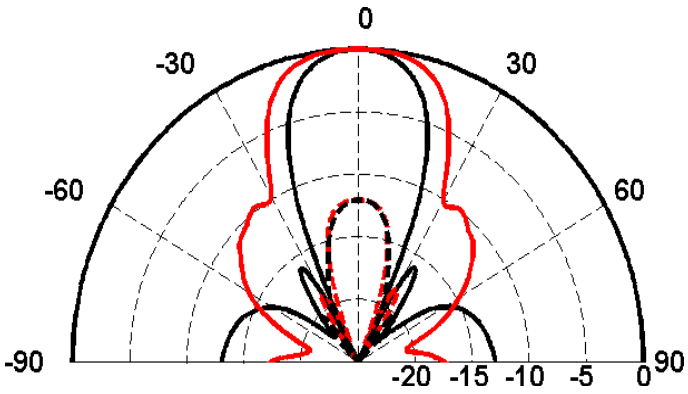


*(a)*

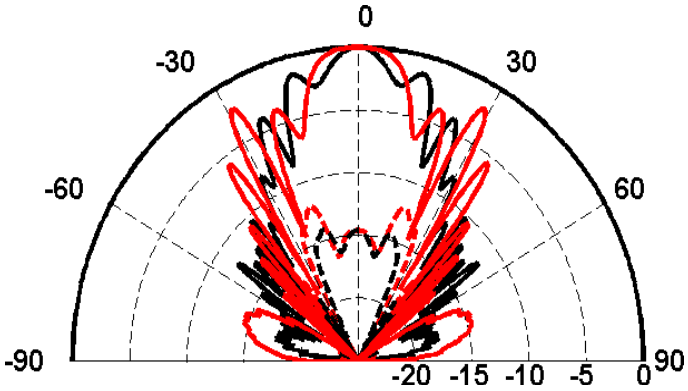


*(b)*

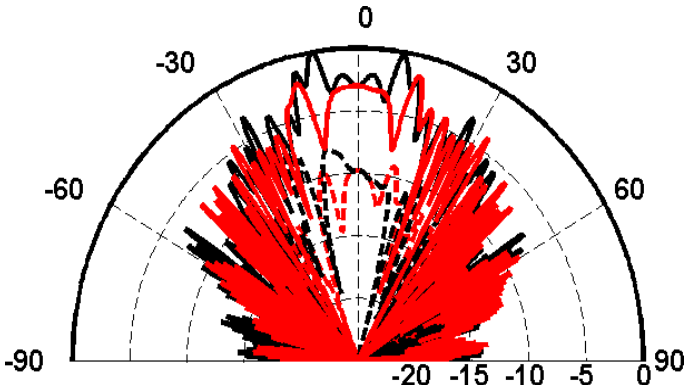


*(c)*

*Figure 16 – Simulated radiation pattern for the DRW antenna with an elliptic lens. E-plane (black) and H-plane (red) co-polar (solid) and cross-polar (dashed) (a) 150 GHz, (b) 300 GHz, and (c) 800 GHz*

Financiado por la Unión Europea NextGenerationEU
GOBIERNO DE ESPAÑA MINISTERIO DE ASUNTOS ECONÓMICOS Y TRANSFORMACIÓN DIGITAL SECRETARÍA DE ESTADO DE TELECOMUNICACIONES E INFRAESTRUCTURAS DIGITALES
Plan de Recuperación, Transformación y Resiliencia
UNICO I+D

## 4.2 Hyper-hemispherical approximation

The geometry of the hyper-hemispherical lens embedded in the DRW antenna is shown in Figure 17.

The wavefront phase error inside the DRW radiation taper is reduced in at least a 1:10 frequency range by forcing TA ray (red) to be parallel to the Z-axis for $\beta_{sc} = 45º$. A hyper-hemispherity of 1 mm is achieved considering a value of $q = \sqrt{\frac{\varepsilon_{ant}}{\varepsilon_{sc}}} = 0.54$ and $\Delta Z = 0.7$ mm for a lens with a radius $R = 2$ mm.

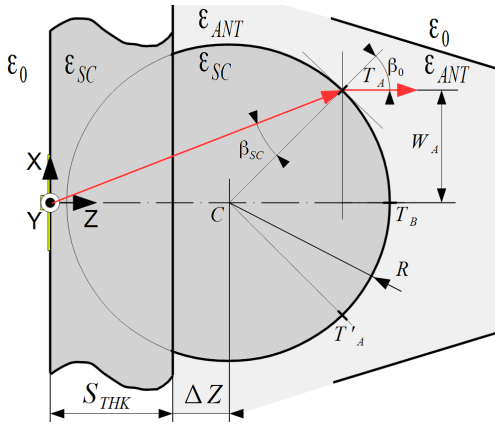


Figure 17 – Geometry of the embedded hyper-hemispherical planar lens.

The simulated E-field distribution inside the DRW antenna with this lens observed in Figure 18 are similar to those achieved with the elliptic lens at frequencies where $W_{ROD} >> \lambda_{DRW}$. Although most of the power is radiated along the main lobe at $\theta = 0º$, there are still side lobes caused by higher order modes at higher frequencies.

Financiado por la Unión Europea NextGenerationEU
GOBIERNO DE ESPAÑA MINISTERIO DE ASUNTOS ECONÓMICOS Y TRANSFORMACIÓN DIGITAL SECRETARÍA DE ESTADO DE TELECOMUNICACIONES E INFRAESTRUCTURAS DIGITALES
Plan de Recuperación, Transformación y Resiliencia
UNICO I+D

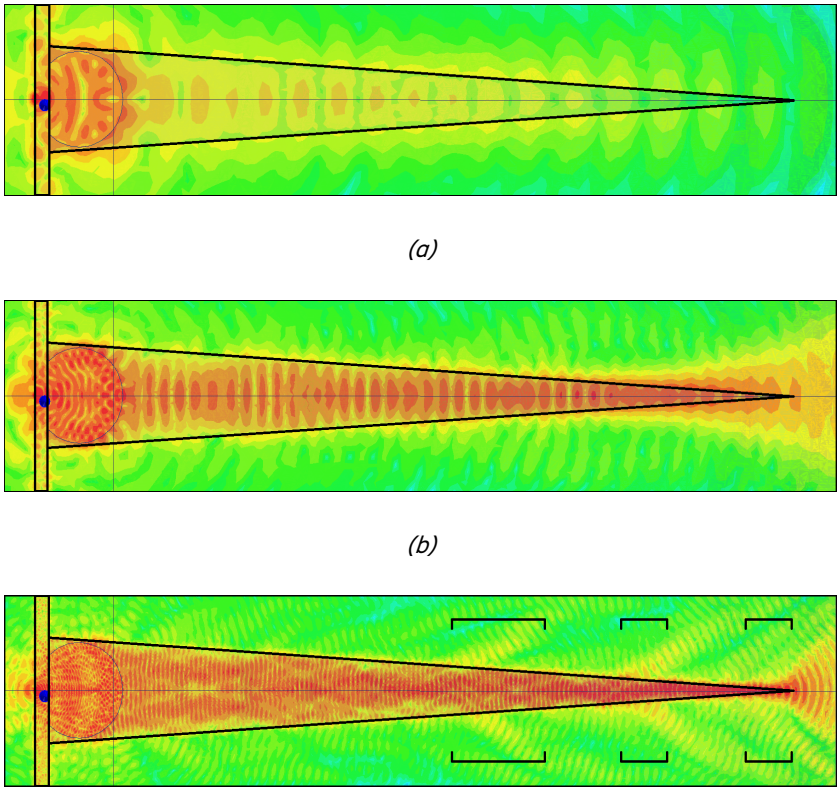

*(a)*

*(b)*

*(c)*

*Figure 18 – Simulated E-field distribution [log(V/m)] on XZ plane for a hyper-hemispherical lens at (a) 150 GHz, (b)300 GHz, and (c) 800 GHz*

Many secondary lobes of comparable levels to the main lobe are appreciated in the radiation patterns in Figure 19 as not all the power is radiated at the DRW antenna tip, and a degradation in the XPD is observed at higher frequencies. Although these results are worse than those obtained with an elliptical lens, a hyper-hemispheric design is preferable as it is easier and more cost-effective to manufacture.

Financiado por la Unión Europea NextGenerationEU
GOBIERNO DE ESPAÑA MINISTERIO DE ASUNTOS ECONÓMICOS Y TRANSFORMACIÓN DIGITAL SECRETARÍA DE ESTADO DE TELECOMUNICACIONES E INFRAESTRUCTURAS DIGITALES
Plan de Recuperación, Transformación y Resiliencia
UNICO I+D

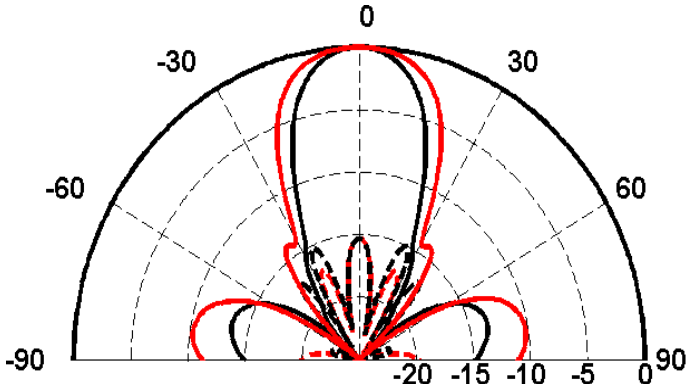


*(a)*

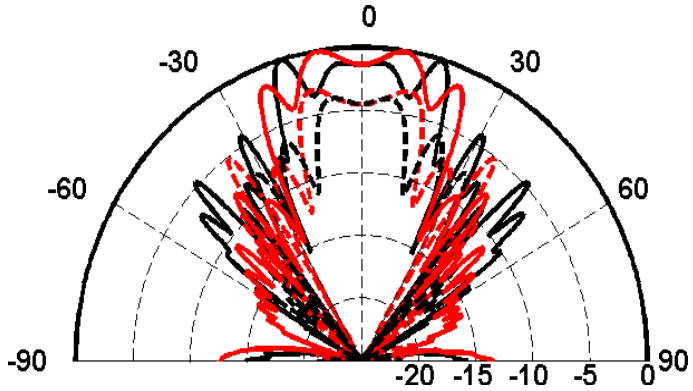


*(b)*

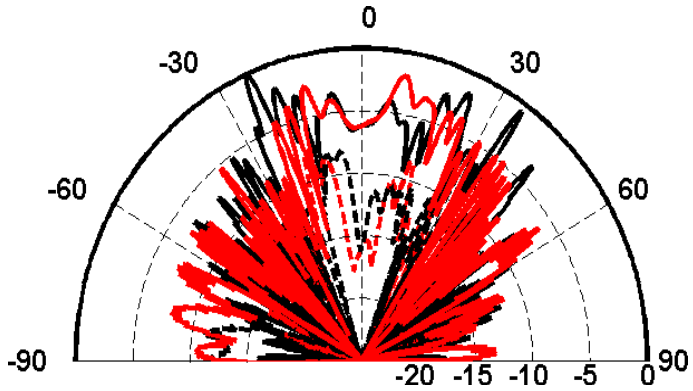


*(c)*

*Figure 19 – Radiation pattern for the DRW antenna with the hyper-hemispheric lens. E-plane (black) and H-plane (red) co-polar (solid) and cross-polar (dashed) (a) 150 GHz, (b) 300 GHz, and (c) 800 GHz*

Financiado por la Unión Europea NextGenerationEU
GOBIERNO DE ESPAÑA MINISTERIO DE ASUNTOS ECONÓMICOS Y TRANSFORMACIÓN DIGITAL SECRETARÍA DE ESTADO DE TELECOMUNICACIONES E INFRAESTRUCTURAS DIGITALES
Plan de Recuperación, Transformación y Resiliencia
UNICO I+D

## 4.3 Low frequency proof-of-concept

A low-frequency proof-of-concept is validated by manufacturing and comparing the measurement results at 25 GHz of an E-tapered polypropylene ($\varepsilon_r$ = 2.2) DRW antenna with and without planar lens. The dimensions of the rod are defined to $L_{TAPER} = 190$ mm and $W_{ROD} = 22$ mm to achieve single-mode propagation in the 6-12 GHz band. A high-permittivity (AD-1000, $\varepsilon_r$ = 10) substrate is used to manufacture an elliptic lens with $q$ = 0:47 and $f = 15$ mm. Higher-order modes are excited using a WR-28 rectangular waveguide without matching taper.

Figure 20 shows the measured radiation patterns of these prototypes at 25 GHz. Destructive interference is produced in the homogeneous DRW antenna as a null in the Z-axis is observed, while a pronounced main lobe along the $\theta$ = 0º direction can be achieved when introducing the lens. The transmission of these antennas in Figure 21, measured using a reference horn, shows that the lens eliminates the nulls of the DRW antenna at 25 and 32 GHz, thereby extending the operation band beyond 30 GHz.

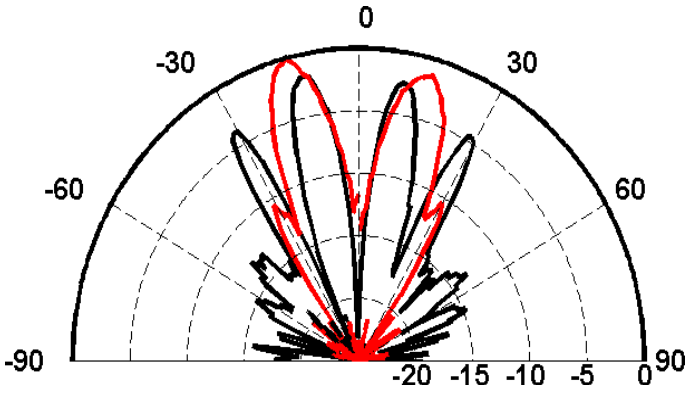


*(a)*

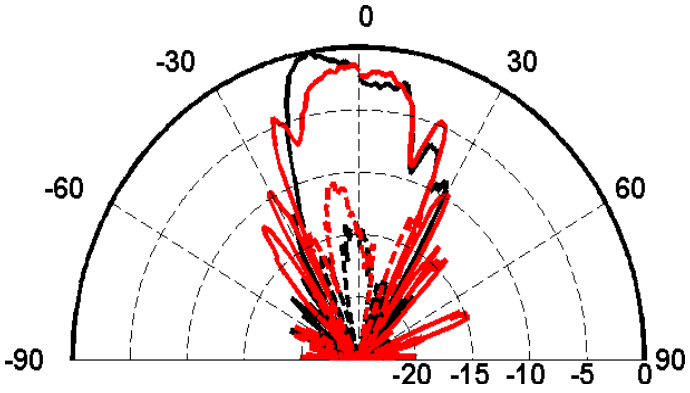


*(b)*

*Figure 20 – Measured radiation pattern with higher-order modes in the rod. E-plane (black) and H-plane (red) co-polar (solid) and cross-polar (dashed) (a) Without planar lens (b) With planar lens*

Financiado por la Unión Europea NextGenerationEU
GOBIERNO DE ESPAÑA MINISTERIO DE ASUNTOS ECONÓMICOS Y TRANSFORMACIÓN DIGITAL SECRETARÍA DE ESTADO DE TELECOMUNICACIONES E INFRAESTRUCTURAS DIGITALES
Plan de Recuperación, Transformación y Resiliencia
UNICO I+D

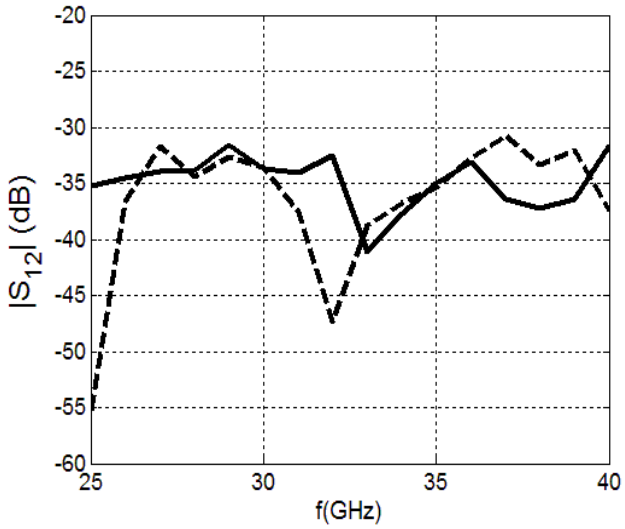


*Figure 21 – Measured |S12| parameter with higher-order modes in the rod. Without lens (solid) and with lens (dashed)*

# 5 Conclusion

DRAs are a high-efficiency, cost-affordable and easy to fabricate alternative to silicon lenses for broadband detectors.

A DRA prototype has been assembled to a photomixing based *n-i-pn-i-p* terahertz source. Radiation pattern measurements at 137 GHz and 150 GHz have been provided for two different samples.

A solution for increasing the band of DRAs has been proposed. Due to the extremely wideband achieved, the lens-based rods designs are electrically large in the E-plane (XZ-plane) for the higher frequencies, which is undesirable in array configurations. They are compacts in the H-plane (YZ-plane), so they can be used for single-plane electronic steerable arrays. Two different lens design strategies have been proposed and compared via full-wave simulations. The concept has been validated through measurements in a low-frequency proof-of-concept.

# 6 Works Cited

[1] "Evolution of Non-Terrestrial Networks From 5G to 6G: A Survey (ieee.org)" Retrieved from: https://arxiv.org/abs/2103.09156

[2] "Non-Terrestrial Network Advantages, Challenges, and Applications" Retrieved from: https://arxiv.org/abs/2103.09156

[3] "Non-Terrestrial Networks (NTN) (3gpp.org)" Retrieved from: https://www.3gpp.org/technologies/ntn-overview

Financiado por la Unión Europea NextGenerationEU
GOBIERNO DE ESPAÑA MINISTERIO DE ASUNTOS ECONÓMICOS Y TRANSFORMACIÓN DIGITAL SECRETARÍA DE ESTADO DE TELECOMUNICACIONES E INFRAESTRUCTURAS DIGITALES
Plan de Recuperación, Transformación y Resiliencia
UNICO I+D

[4] "5G from Space: An Overview of 3GPP Non-Terrestrial Networks" Retrieved from: https://arxiv.org/abs/2103.09156

[5] "Connecting the world with 5G NTN" Retrieved from: https://arxiv.org/abs/2103.09156

[6] "ATSSS in 5G networks" Retrieved from: https://arxiv.org/abs/2103.09156

[7] 5G-ACIA "5G-ACIA 5G Non-Public Networks for Industrial Scenarios" https://5g-acia.org/wp-content/uploads/5G-ACIA_5G_Non-Public_Networks_for_Industrial_Scenarios_09-2021.pdf

[8] "Terminology for Benchmarking Network-layer Traffic Control Mechanisms" RFC 4689 RFC 4689 - Terminology for Benchmarking Network-layer Traffic Control Mechanisms (ietf.org)

[9] "About IMDEA Networks" Retrieved from: https://networks.imdea.org/about-imdea-networks/

[10] "About 5Tonic" Retrieved from: https://www.5tonic.org/